#### RESEARCH



# Application of a dual-modality colorimetric analysis method to inkjet printing lateral flow detection of *Salmonella typhimurium*

Ya-Ching Yu<sup>1</sup> · Zhijian Wang<sup>1</sup> · Xiaoyu Ji<sup>2</sup> · Eric Jacob Williamson<sup>3</sup> · Hansel Mina Cordoba<sup>4</sup> · Ana M. Ulloa-Gomez<sup>1</sup> · Amanda J. Deering<sup>4</sup> · George T.-C. Chiu<sup>3</sup> · Jan P. Allebach<sup>2</sup> · Lia A. Stanciu<sup>1,5</sup>

Received: 8 July 2024 / Accepted: 11 August 2024 / Published online: 23 August 2024 © The Author(s), under exclusive licence to Springer-Verlag GmbH Austria, part of Springer Nature 2024

#### **Abstract**

Lateral flow assay (LFA) color signal quantification methods were developed by utilizing both International Commission on Illumination (CIE) LAB (CIELAB) color space and grayscale intensity differences. The CIELAB image processing procedure included calibration, test, control band detection, and color difference calculation, which can minimize the noise from the background. The LFA platform showcases its ability to accurately discern relevant colorimetric signals. The rising occurrence of infectious outbreaks from foodborne pathogens like *Salmonella typhimurium* presents significant economic, healthcare, and public health risks. The study introduces an aptamer-based lateral flow (ABLF) platform by using inkjet printing for specially detecting *S. typhimurium*. The ABLF utilized gold-decorated polystyrene microparticles, functionalized with specific *S. typhimurium* aptamers (Ps-AuNPs-ssDNA). The platform demonstrates a detection limit of 10<sup>2</sup> CFU mL<sup>-1</sup> in buffer solutions and 10<sup>3</sup> CFU mL<sup>-1</sup> in romaine lettuce tests. Furthermore, it sustained performance for over 8 weeks at room temperature. The ABLF platform and analysis methods are expected to effectively resolve the low-sensitivity problems of the former LFA systems and to bridge the gap between lab-scale platforms to market-ready solutions by offering a simple, cost-effective, and consistent approach to detecting foodborne pathogens in real samples.

Keywords Lateral flow biosensor · CIELAB · Aptamer · Salmonella typhimurium · Inkjet printing

#### Introduction

Traditional lateral flow assays (LFAs) are highly useful and are applied in various fields, but face significant challenges such as limited sensitivity, which hinder their practical application, particularly in the rapid detection of foodborne pathogens. The introduction of advanced LFA

- ☐ Lia A. Stanciu lstanciu@purdue.edu
- School of Materials Engineering, Purdue University, 701 West Stadium Ave., West Lafayette, IN 47907, USA
- School of Electrical and Computer Engineering, Purdue University, 465 Northwestern Ave, West Lafayette, IN 47907, USA
- School of Mechanical Engineering, Purdue University, 585 Purdue Mall, West Lafayette, IN 47907, USA
- Department of Food Science, Purdue University, 745 Agriculture Mall Dr, West Lafayette, IN 47907, USA
- <sup>5</sup> Bindley Bioscience Center, Purdue University, 1203 W State St, West Lafayette, IN 47907, USA

image analysis and quantification methods that utilize both International Commission on Illumination (CIE) LAB (CIELAB) color space and grayscale intensity differences to enhance sensitivity offer a potential solution for enhancing the performance of these assays [1]. These methods allow for distinguishing signals that are difficult to resolve by the naked eye, thus expanding system sensitivity. The image processing procedures, including calibration, test, control band detection, and color difference calculation, minimize background noise and accurately discern relevant colorimetric signals.

The global burden of foodborne infectious outbreaks remains a significant public health concern, affecting over 48 million people annually with a mortality rate of 6.25% [2]. According to the World Health Organization (WHO), foodborne pathogens are responsible for 600 million cases and 420,000 deaths worldwide each year [3]. Pathogens such as *Escherichia coli*, *Salmonella* spp., *Staphylococcus aureus*, *Listeria* spp., *Campylobacter* spp., *Shigella* spp., and *Bacillus cereus* pose a major challenge to both public health and the food industry, resulting in

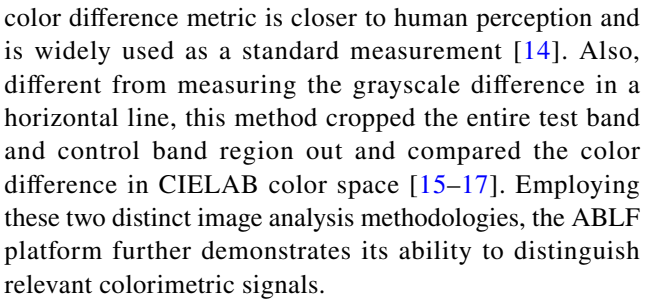


significant economic losses [2]. Among these foodborne pathogens, *Salmonella* spp., which is predominantly transmitted through fresh-cut vegetables and dairy, is estimated to be responsible for approximately 85% of worldwide foodborne diseases. *Salmonella* contamination posed a major public health concern around the globe and led to over 100,000 deaths and substantial economic costs annually [4].

Lateral flow assays (LFAs) are recognized as pointof-care devices that meet the Affordable, Sensitive, Specific, User-friendly, Rapid/Robust, Equipment-free, and Deliverable (ASSURED) criteria [5]. It makes them effective for on-site analyte detection with quick qualitative or semi-quantitative results [5]. Recently, aptamers have gained a lot of attention as a biorecognition molecular substitute for antibodies. Aptamers possess the ability to adopt three-dimensional structures characterized by high thermodynamic stability, enabling specific binding to desired targets through van der Waals forces, hydrogen bonding, and electrostatic interactions [6]. From a manufacturing perspective, aptamers offer advantages such as low-cost production, ease of synthesis and modification at high scales under controlled conditions, and better shelf life [7]. Consequently, aptamer-based lateral flow (ABLF) assays have become an increasingly researched area, with several studies focusing on pathogens. For instance, one study successfully developed an aptasensing platform for the detection of E. coli O157:H7 and S. typhimurium using microfluidic paper-based devices [8]. Furthermore, various reports have utilized aptasensors specific to certain bacteria, enabling direct interaction with the cell surface for whole-cell bacteria detection without complex preparation procedures [9-12].

Inkjet printing has been instrumental in advancing the development of paper-based bio-analytical devices (PBDs). This technology enhances the production of ABLF assays for detecting foodborne pathogens, offering benefits in terms of accuracy, cost-effectiveness, and sensitivity across various manufacturing scales [9, 13]. Recently, research is focusing on using antibodies, catalytic proteins, and aptamers as bioactive inks. Drop-on-demand (DOD) printing precisely deposits ink droplets at required locations, eliminating runoff. To protect thermally sensitive inks, piezoelectric inkjet printing is employed to avoid ink damage, providing precise printing accuracy and excellent compatibility for bioink applications.

Furthermore, the efficacy of the ABLF platform in detecting *S. typhimurium* was additionally evaluated with a color space image processing method to validate the bacteria detection from the visual perceptual perspective, while still providing a quantitative assessment. Compared to grayscale intensity difference, the CIELAB trichromatic



To date, several reports have focused on ABLF assays for detecting foodborne pathogens [9, 10, 18]. In Lu's study [10], ABLF detected E. coli O157:H7, S. typhimurium, and Staphylococcus aureus using primary and secondary aptamer as a sandwich-type format to capture the target pathogen. Although they achieved a limit of detection (LOD) of 10<sup>3</sup> CFU mL<sup>-1</sup> for S. typhimurium in various food samples, leafy greens were not among them. Moreover, there were no selectivity studies, recovery rates, or manufacturing insights in this particular report. On the other hand, Wu's group [19] evaluated the LFA assay in the milk sample, which is a relatively simpler sample for detection. As for Bhandari's work [20], although a low limit of detection of 0.9 log CFU g<sup>-1</sup> of S. typhimurium was reached in romaine lettuce, this platform required the separation of flagellin from the S. typhimurium for all experiments, which is not practical in the real applications.

In this investigation, we took advantage of the versatility, cost-effectiveness, and stability of ssDNA-based aptamers. These were combined with gold nanoparticles on polystyrene microparticles (Ps-AuNPs) to create an inkjet-printed aptamer-based lateral flow assay for detecting *S. typhimurium*, as shown in Scheme 1. Additionally, we utilized grayscale intensity difference and the CIELAB trichromatic color difference metric for visual validation of bacteria detection and quantitative assessment. To the best of our knowledge, this study introduces the first ABLF platform for specificity testing in romaine lettuce samples. Incorporating comprehensive recovery studies and long-term stability under room-temperature storage conditions, our platform aims to bridge the gap between laboratory research and practical applications.

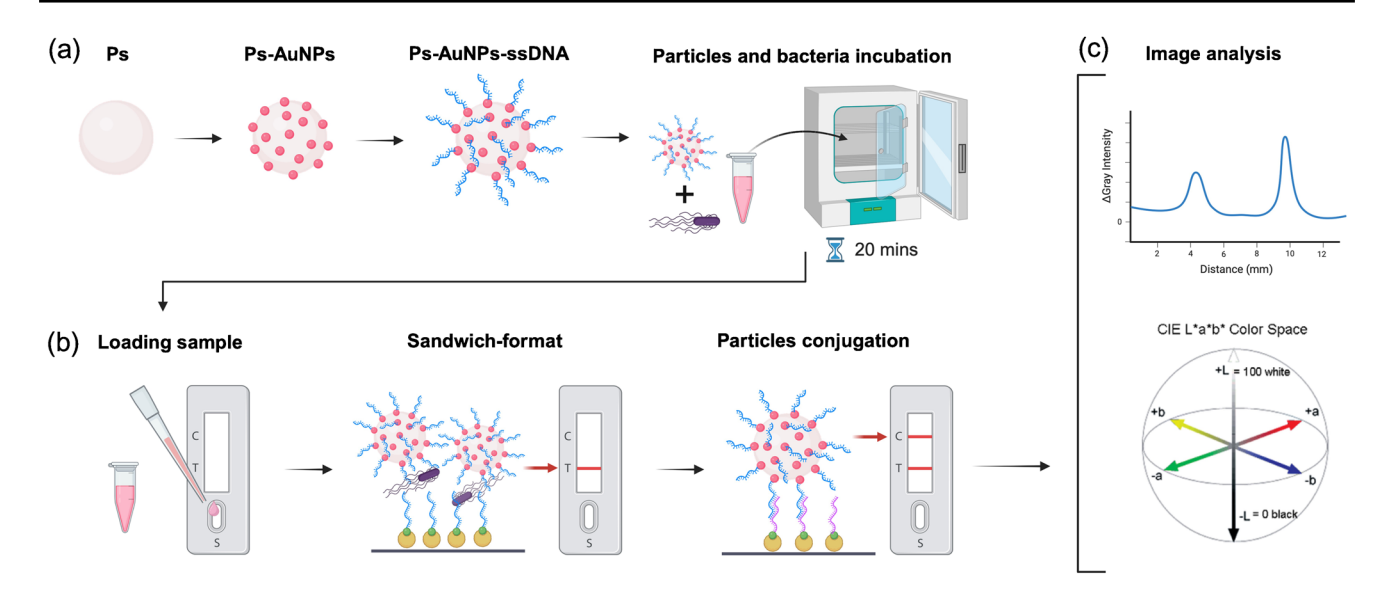
### **Experimental section**

#### Reagents and materials

The following reagents were procured: 0.01 M phosphate buffer solution (pH 7.4 at 25 °C), poly-styrene latex beads (0.46-µm average diameter), gold (III) chloride trihydrate (99.9%), bovine serum albumin (BSA), trisodium citrate dihydrate, nuclease-free water for molecular biology,



Microchim Acta (2024) 191:559 Page 3 of 13 559



**Scheme 1** Graphical illustration of the ABLF construction for *S. typhimurium* detection. **a** The synthesis process of Ps-AuNPs conjugated with aptamer and sample preparation. **b** The schematic of

ABLF detecting pathogens. **c** Test interpretation by two image analysis methods. (Created with BioRender.com)

and TWEEN® 20 from Sigma-Aldrich. Streptavidin was obtained from Thermo Scientific. Laminated cards (60 mm) with FF80 HP nitrocellulose membrane (25 mm NC membrane), Whatman CF1, and Whatman CF5 dipstick pads were acquired from Cytiva. Tris-EDTA buffer (pH 7.5 and 8.0) was sourced from Integrated DNA Technology (IDT). All single-stranded DNA (ssDNA) sequences, normalized to 100 μM in IDTE buffer (pH 8.0), were purchased from Integrated DNA Technology (IDT, Coralville, IA, USA). Below are the modified aptameric sequences used herein, modified from the literature [21]. The aptamer's secondary structure is displayed in Fig. A.1(b) [21].

- Thiolated-ssDNA (Thiol-ssDNA): /5ThioMC6-D/TTT TTT TTT TAC TAT CGC GGA GAC AGC GCG GGA GGC ACC GGG GA
- Biotinylated-ssDNA (B-ssDNA): /5Biosg/TTT TTT TTT TAC TAT CGC GGA GAC AGC GCG GGA GGC ACC GGG GA
- Biotinylated-complementary-ssDNA (B-C-ssDNA): /5Biosg/TTT TTT TTT TCC CCG GTG CCT CCC GCG CTG TCT CCG CGA TAG TAA AAA AA

All glassware was cleaned using Aqua regia solution (a mix of concentrated nitric acid and hydrochloric acid in a 1:3 ratio), thoroughly rinsed with deionized (DI) water, and dried with nitrogen before use. All chemicals employed were of analytical grade.

## Characterization of Ps-AuNPs-ssDNA microparticles and nitrocellulose membrane

Bright-field transmission electron microscopy (TEM), specifically the Tecnai G2 20 (operating at 200 kV with a LaB6 filament, Oxford Instruments), was utilized to image the Ps and Ps-AuNPs microparticles. UV–Visible spectra were obtained using a Spectra Max Plus 384 spectrophotometer (Molecular Devices, Sunnyvale, CA, USA). Zeta potential measurements were performed with a Zetasizer Nano Z (Malvern Instruments Ltd., Westborough, MA, USA). The surface morphology and microstructure of the nitrocellulose membrane, particularly for capturing the Ps-AuNPs and bacteria, were examined using scanning electron microscopy (SEM; S-4800, Hitachi).

#### **Synthesis of Ps-AuNPs**

To produce gold-based microparticles, 100  $\mu$ L of polystyrene beads (Ps) with an average diameter of approximately 0.46  $\mu$ m from the original stock solution was mixed with 20 mL of DI water and stirred at 300 rpm for 10 min. Subsequently, 26 mL of DI water and 60  $\mu$ L of 254 mM gold (III) chloride trihydrate (HAuCl<sub>4</sub> · 3H<sub>2</sub>O,  $\geq$  99.9%) in DI water were added to the Ps solution and stirred for 5 min at room temperature (RT). The mixture was stirred for 30 min, at a temperature near the boiling point, with the hot plate temperature being set to 190 °C. Subsequently, 55 mg of trisodium citrate dihydrate was added to the solution, resulting in final concentrations



**559** Page 4 of 13 Microchim Acta (2024) 191:559

of 0.33 mM and 4.08 mM for gold (III) chloride trihydrate and trisodium citrate dihydrate, respectively. Heterogeneous nucleation occurred as a result of the lower energy barrier provided by the polystyrene beads, leading to the formation of gold nanoparticles on the surface of polystyrene. The solution was stirred for an additional 20 min. The formation of gold nanoparticle-decorated polystyrene microparticles (Ps-AuNPs) was indicated by the solution turning pink. After synthesis, the solution was cooled in ice and stored at 4 °C. Excess reactants were removed via centrifugation (4000 rpm, 35 min) at 4 °C, and the Ps-AuNPs pellets were then resuspended in DI water by vortexing.

### **Aptamer functionalization**

Thiol-ssDNA was functionalized on the Ps-AuNPs based on the previously reported method with some modifications [22]. Initially, thiol-ssDNA aliquots were removed from 4 °C and heated at 95 °C for 3 min in a heat block, and then quickly cooled. Following this, 420 µL of thiolssDNA was activated by mixing it with 420 µL of freshly prepared 10 mM TCEP, and the mixture was incubated at room temperature for 1 h. Twenty-one milliliters of concentrated Ps-AuNPs solution was mixed with this solution and stirred at 150 rpm, covered with an opaque box, at room temperature for 16 h. To enhance aptamer loading on the AuNPs surface, 105 µL of 1 M NaCl and 420 µL of 500 mM Tris-acetate buffer (pH 8.2) were gradually added, and the mixture was stirred for an additional 24 h. The particles were then centrifuged at 4000 rpm for 35 min to remove unbound ssDNA. The resulting red pellet was resuspended in rinsing buffer (20 mM Na<sub>3</sub>PO<sub>4</sub>, 5% BSA, 0.25% Tween-20, and 10% sucrose) to an optical density (OD) of 2.4 and stored at 4 °C until use.

# Bioink preparation and lateral flow test strip assembly

For bioink preparation, 300  $\mu$ L of 2 mg mL<sup>-1</sup> streptavidin was mixed with 150  $\mu$ L of either biotinylated capture probe (B-ssDNA) or biotinylated control probe (B-C-ssDNA), both at 100  $\mu$ M in IDTE pH 8.0. This mixture was incubated at room temperature for 1 h. Subsequently, 3 mL of PBS was added, and excess aptamer was removed via ultrafiltration (30 kDa) by centrifuging at 10,000 rcf for 10 min at 4 °C. This filtration step was repeated twice, after which the conjugates in the filter were collected through centrifugation. The conjugates were then diluted to 600  $\mu$ L with PBS and stored at 4 °C for later use in inkjet printing. Lateral flow test strips were assembled with a 3-mm overlap between each layer to facilitate sample flow from the sample pad to the absorbent pad. The strips were cut to 60 mm in length and 3 mm in width. Preliminary tests showed that the FF80 HP

nitrocellulose membrane provided better fluid transport than the HF 120 solution, without any trapping effect, leading to its selection for subsequent experiments.

# Inkjet printing for aptamer-based lateral flow test strip

Piezoelectric drop-on-demand inkjet printing was employed to apply control and test lines onto the NC membrane using a PipeJet® nanodispenser and a Biofluidix controller (Biofluidix, Freiburg, Germany). After optimizing the print settings for this specific ink, the nanodispenser was adjusted to an 80% piston stroke, a piston velocity of 100 µm s<sup>-1</sup>, and a frequency of 100 Hz, with the nozzle positioned 1 mm above the nitrocellulose membrane, as shown in Fig. A.1(a). Each deposition site received a single ink droplet. The pixel pitch, the distance between adjacent droplets, was set at 0.25 mm for both control and test solutions. For both lines, spaced 5 mm apart, multiple layers were deposited to ensure adequate signal strength. Each layer was printed and dried with a hot air gun before adding the next. Lines were fully printed and dried before the next line's printing began, ensuring even drying. After printing, the ABLF sheet was dried at 37 °C for 2 h, cut into 3-mm wide strips, and stored at 4 °C.

#### **Bacteria culture preparation**

Microorganisms, including E. coli O157:H7, E. coli K12, Salmonella typhimurium ATCC 14028, and Listeria monocytogenes, were obtained from frozen stocks at Purdue University's Food Science Department. Fresh cultures were first plated on agar and incubated overnight. A single colony from each plate was then transferred to 30 mL of sterile Luria-Bertani (LB) media or Brain Heart Infusion (BHI) media (BD Difco<sup>TM</sup>) and cultured in a temperaturecontrolled orbital shaker at 35 °C and 160 rpm for 20 h. The fully grown bacteria were centrifuged three times (6000 rpm, 5 min) and resuspended in 30 mL of 0.1M PBS buffer solution (pH 7.0). Bacterial concentrations in the stock culture were determined by selective plating on MacConkey Sorbitol Agar, XLT-4 agar, and Modified Oxford agar (all BD Difco $^{TM}$ ) for specific growth of the respective E. coli strains, S. typhimurium, and L. monocytogenes.

#### **Optical detection assay**

The *S. typhimurium* culture underwent serial dilution in PBS buffer, resulting in known concentrations ranging from  $10^1$  to  $10^7$  CFU mL<sup>-1</sup>. Subsequently,  $30 \mu L$  of the Ps-AuNPs-ssDNA solution was mixed with  $10 \mu L$  of the bacterial solution and incubated at 37 °C for 20 min. The 3:1 ratio between Ps-AuNPs-ssDNA and the bacterial solution was determined by the preliminary test, and it showed the



Microchim Acta (2024) 191:559 Page 5 of 13 **559** 

highest signal with optimum aptamer amount conjugating with bacteria. After incubation, the mixture was applied to the sample pad of each test strip, which was then allowed to dry for 10 min before proceeding with image acquisition and analysis. To assess the platform's specificity, this process was repeated using potential high-concentration interferents (bacterial interferents at  $10^6$  CFU mL<sup>-1</sup>). PBS buffer served as a negative control (0 CFU mL<sup>-1</sup>). To assess the reproducibility of the detection in solution, three replicates were compared per condition.

### Real sample testing

Romaine lettuce, sourced from the Walmart store in West Lafayette, IN, USA, served as the matrix for food sample testing. Non-organic lettuce was purchased without pretreatment and stored at 4 °C for up to 2 days before experiments. To prevent interference from pesticides and soil, the outer two to three leaves were removed. Two to three inner leaves were then selected and weighed to 25 g per sample. These lettuce samples were spiked and inoculated with 1 mL of 10<sup>7</sup> CFU mL<sup>-1</sup> bacterial suspension. The spiked samples were cultured in a biosafety cabinet at room temperature for 2 h, followed by homogenization in 225 mL of sterile PBS buffer (pH 7.0) using the blending method. The homogenized samples were then placed in sterile stomacher bags (710 mL, Whirl-Pak® Homogenizer Blender Filter Bag) to remove fibers and debris. Serial dilutions of the filtered solution were used to create various target concentrations ranging from 10<sup>2</sup> to 10<sup>5</sup> CFU mL<sup>-1</sup> for ABLF assays and spike-recovery tests. All experiments were conducted in triplicate in real sample tests.

### Image acquisition and grayscale difference analysis

To control illumination conditions, ABLF strips were placed in a photo booth for image capture. Images were acquired within 10 min of each measurement using a Nikon Z fc camera with a Z DX 18-140mm zoom lens (1/250 s, 70 mm F5.3, ISO 160). The images were then processed with ImageJ software, converting them into 8-bit grayscale. The intensity values of the test and control lines were determined by plotting their profiles. To quantify the grayscale values across different strips, background values from each strip were subtracted from the original values to eliminate noise effects. The intensities of the test and control lines were recorded, with all tests run in triplicate. Spectral and intensity data were analyzed using OriginLab 2022 (Northampton, MA, USA). All the Error bars presented in this study are the standard deviation based on at least three independent measurements. The limit of detection (LOD) was calculated by where the signal exceeds the average of the blank signal plus three times the standard deviation of the blank.

#### **CIELAB** color space analysis

The procedure of CIELAB image processing included calibration, test and control band detection, and color difference calculation. The calibration step aligned the test strips horizontally based on Hough Line detection [23]. We plotted the average grayscale color in the horizontal direction from the aligned test image, the local valleys were locations of the test band and control band, as shown in Fig. A.2. According to the size of the ABLF platform, the width of the test band and control band is one-third of the height. The extracted test region and control region are between green lines. The background color was extracted from the middle of the test band and control band, which is the region between the red lines in Fig. A.2.

The CIELAB color difference metric is shown below:

$$\Delta E(i,j) = \sqrt{\left(L(i,j) - L_{avg}\right)^2 + \left(A(i,j) - A_{avg}\right)^2 + \left(B(i,j) - B_{avg}\right)^2}$$

The  $L_{avg}$ ,  $A_{avg}$ , and  $B_{avg}$  are the average LAB colors of the background region. L(i,j), A(i,j), and B(i,j) are the pixelwise L, A, and B channel colors of the test and control band image. The metric output  $\Delta E$  is an image representing the color difference between background and test and control band. The "DeltaE" value indicates the average intensity of the  $\Delta E$  image of the test band.

#### **Results and discussion**

#### **Detection mechanism**

This study utilized the stability of biocapture molecules, biotinylated aptamer (B-ssDNA), and complementary biotinylated aptamer (B-C-ssDNA), and explored their integration as "bioinks" in a noncontact inkjet printing technique. The aptamer-based lateral flow (ABLF) developed herein utilized a well-established sandwich mechanism to detect foodborne pathogens in such paper-based devices and focused on Salmonella typhimurium. The bacteriacontaining sample was first conjugated with gold-decorated polystyrene microparticles (Ps-AuNPs) functionalized with thiolated-ssDNA aptamers specific to Salmonella typhimurium (Scheme 1a). These aptamers bind to the target bacteria, forming an aptamer-bacteria complex. This sample was then applied to the sample pad of the ABLF and migrated through the strip in a uniform flow. As this sample continued to migrate along the nitrocellulose membrane (NC), this aptamer-bacteria complex reached the test line (Scheme 1b). Here, biotinylated-ssDNA (B-ssDNA) had been immobilized, capturing the complex through a biotin-streptavidin interaction and forming a sandwich structure. Any unbound



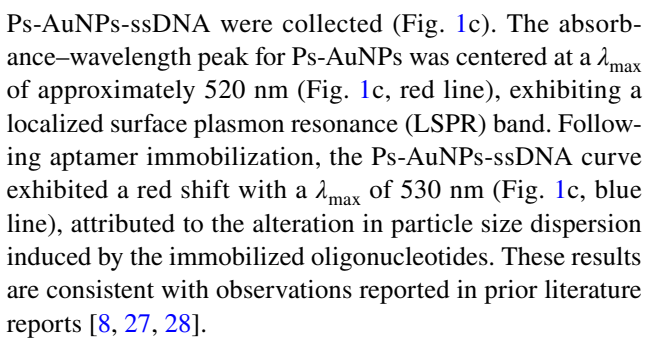
Ps-AuNPs-ssDNA complexes continued to migrate to the control line, where complementary biotinylated-ssDNA (B-C-ssDNA) had been immobilized, capturing excess conjugates and serving as an internal control to confirm the assay's proper function. The presence of Salmonella typh*imurium* is indicated by the appearance of colored lines at both the test and control regions. The intensity of the test line correlates with the concentration of the target bacteria, while the control line provides a qualitative check for assay validity. The process concluded with image capture and analysis of the dried sample, using a Nikon Z fc camera (Scheme 1c). In a lateral flow assay (LFA) like the one presented here, the aptamer immobilized on the nitrocellulose (NC) membrane captures bacteria from the sample as it migrates through the test strip. This immobilization ensures that the bacteria are localized in a specific region, leading to the formation of a clear sandwich complex with the test line aptamer.

#### **Materials characterization**

Although AuNPs have played a crucial role in biosensing and diagnostics due to their straightforward synthesis, facile functionalization, and signal amplification capabilities [24, 25], they exhibited lower stability in real-sample detection, impacting sensitivity and colorimetric quantification ability [26]. To address this, core–shell composites through the in situ synthesis of AuNPs on polystyrene beads (Ps), as shown in Fig. 1a, were applied in this study to achieve controlled AuNP size and precise colorimetric detection. This approach was intended to mitigate the limitations of bare AuNPs, offering improved stability and selectivity in biosensing applications [8, 9, 27, 28]. The study validated the monodispersity and controlled growth of AuNPs using transmission electron microscopy (TEM), as shown in Fig. 1b, offering insights into the self-assembly of AuNP-decorated Ps beads. Analysis with ImageJ software revealed that the average size of Ps beads was 397.89 nm with a standard deviation (SD) of  $\pm 9.55$  and a relative standard deviation (RSD) of 2.40%. For AuNPs, the average size was 12.32 nm with an SD of  $\pm 1.83$  and an RSD of 14.85%.

Histograms of the Ps and Ps-AuNP sizes in Fig. A.3 demonstrated that the uniform size of AuNPs on Ps beads provided a consistent space for thiolated-ssDNA functionalization. Moreover, the monodispersity of AuNPs on Ps beads ensured similar aptamer immobilization on each Ps-AuNP microparticle, leading to reproducible detection performance. These findings align with other literature reports where gold-decorated polystyrene particles were used in biosensors for pathogen or cardiac troponin T detection [27, 28].

To further validate the aptamer immobilization on Ps-AuNPs microparticles, UV-vis spectra of Ps-AuNPs and



Zeta potential measurements were conducted to assess surface charge and colloidal stability at various stages of microparticle synthesis, as shown in Fig. 1d. Initially, bare Ps microparticles presented a negatively charged surface, with a potential of  $-52.63 \pm 0.85$  mV, due to sulfate groups attached to the Ps's surface during polymerization, which served as an electrostatic stabilizer [29]. The incorporation of AuNPs into Ps resulted in a minor decrease in the zeta potential to  $-61.40 \pm 1.11$  mV, indicating the existence of negatively charged citrate ions on the surfaces of the AuNPs. The immobilization of thiolated aptamer on the AuNPs' surface further decreased the negative zeta potential to  $-46.66 \pm 1.71$  mV, as the aptamers partially covered the citrate-capped surface of the AuNPs. The introduction of steric stabilization among the microparticles contributed to enhanced colloidal stability. Importantly, all zeta potential values remained above  $\pm 30$  mV, indicating a high level of colloidal stability in the resulting microparticle solution.

#### **Optimization of assay conditions**

In the optimization of the aptamer-based lateral flow assay for *S. typhimurium* detection, the concentration of the microparticle solution was assessed by testing various optical densities (OD), as measured by the UV–vis spectra depicted in Fig. A.4(a). Microparticle solutions with OD values ranging from 0.3 to 3.0 were applied to the sample pad and transported to the absorbent pad. The optimal concentration for efficient ABLF flow, determined through profile analysis shown in Fig. A.4(b), was found to be OD = 2.4 and was used in subsequent experiments.

Different aptameric DNA sequences were tested for specificity to foodborne pathogens, including *E. coli* O157:H7, *S. typhimurium*, and *L. monocytogenes*, and one aptamer (Fig. A.1(b)) was eventually selected based on its performance towards *S. typhimurium* detection. In literature [30], polyT (20 bases) consisting of 20 thymine nucleotides is frequently employed as a spacer in aptamer design because it serves as a flexible and unstructured linker, preventing steric hindrance and unwanted interactions. As the polyT is attached to the Au surface, the available room for the lengthy DNA chains diminishes, prompting them to orient into a more upright conformation [31]. Therefore, the 5' end of the selected aptamer



Microchim Acta (2024) 191:559 Page 7 of 13 **559** 

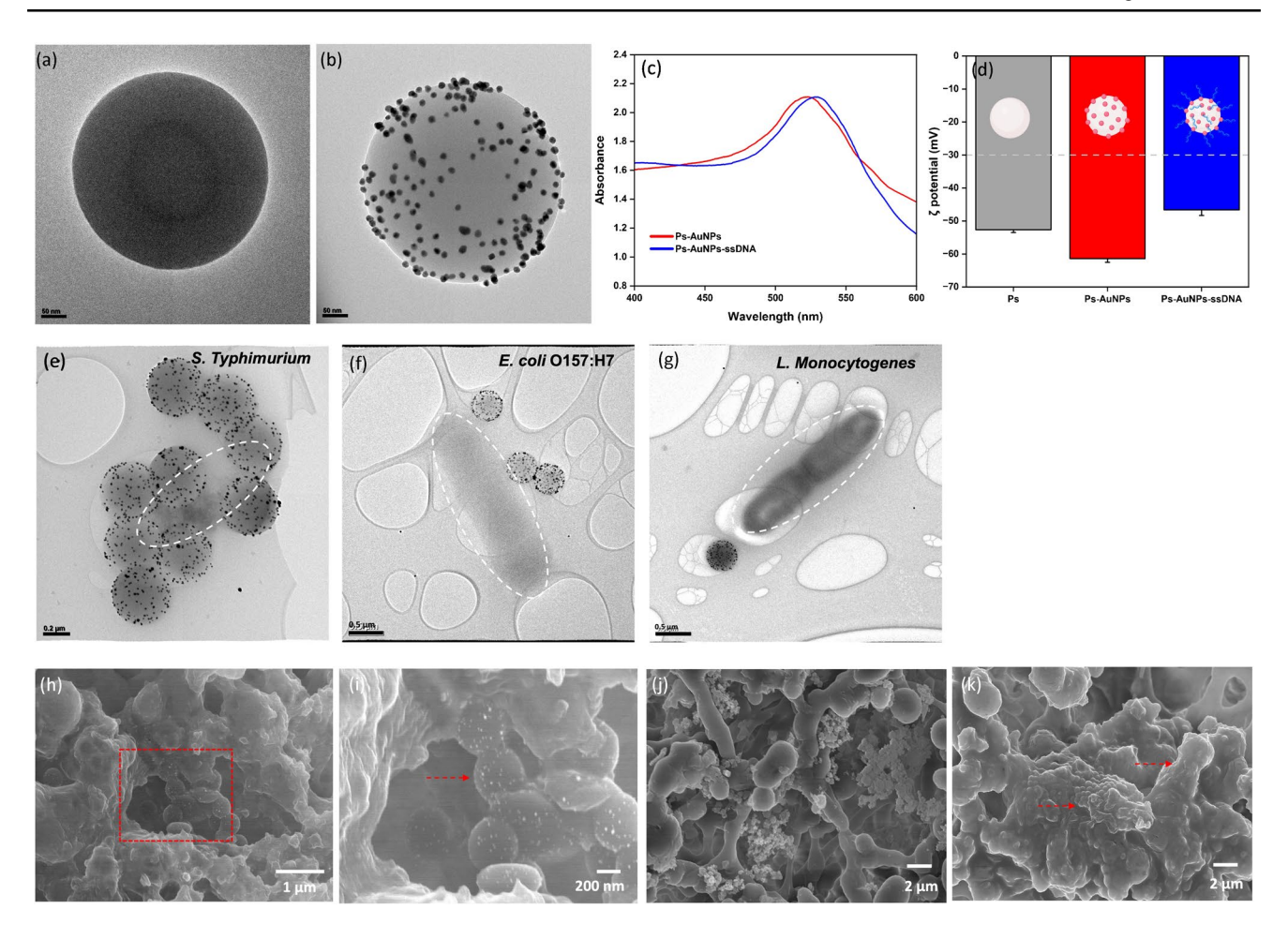


**Fig. 1** TEM images of **a** Ps and **b** Ps-AuNPs microparticles. **c** UV–Vis spectra Ps-AuNPs and Ps-AuNPs-ssDNA. **d** Zeta-potentials of Ps, Ps-AuNPs, and Ps-AuNPs-ssDNA. TEM images for aptamer affinity examination showed **e** Ps-AuNPs-ssDNA microparticles incubated with *S. typhimurium*. The labeled area indicated the contour of *S. typhimurium* which was surrounded by the microparticles. Compared with no-target pathogens **f** *E. coli* O157:H7 and **g** *L. monocytogenes*, aptamer on the microparticles showed lower affinity to cover

the bacterium surface. Next, selective top-view of SEM images of  $\bf h$  Ps-AuNPs-ssDNA microparticles on the control line.  $\bf i$  The zoomin image of the marked area in  $\bf h$ , and the red arrow pointed out the captured microparticles.  $\bf j$  Original NC membrane morphology.  $\bf k$  After the sample flowed through the ABLF strip,  $\it S.$  typhimurium was caught by the microparticles and aptamer on the NC membrane. The red arrows pointed out the captured  $\it S.$  typhimurium

was attached with polyT (20) and functionalized with the thiol group for its immobilization on AuNPs. However, due to the conformational changes resulting from the polyT, we speculate that its secondary structure may have been altered in such a way that the affinity to bacteria changed, which resulted in its specificity towards *S. typhimurium* rather than *L. monocytogenes*, for which it had originally been designed [27]. In the preliminary results, by using the drop-casting method to prepare the control line and test line, the microparticle solution was mixed with three bacteria with 10<sup>7</sup> CFU mL<sup>-1</sup> concentration. The results show that *S. typhimurium* exhibited the highest affinity with thiol-ssDNA, as illustrated in Fig. A.5.

To further confirm the aptamer affinity to *S. typhimu-rium*, the Ps-AuNPs-ssDNA microparticle solution was mixed with 10<sup>7</sup> CFU mL<sup>-1</sup> of *E. coli* O157:H7, *S. typhimurium*, and *L. monocytogenes* in a 3:1 ratio, and then

incubated for 20 min. A volume of 3  $\mu$ L of the mixing solution was deposited on the TEM grids and dried. The aptamer affinity binding with *S. typhimurium* was observed in the TEM images, as shown in Fig. 1e and f. Compared with the other two bacteria, *S. typhimurium* demonstrated the best coverage around the bacterial cell, and flagellin also exhibited high attraction to be captured by microparticles. As for *E. coli* O157:H7 and *L. monocytogenes*, a few microparticles were attached to the surface probably because of the hydrogen bonding between aptamer and bacteria surface, as depicted in Fig. 1g and h [6].

### Inkjet printing platform

The printing media's viscosity was uniformly measured before printing, registering at approximately 1.35 mPa·s for both test



and control solutions. Despite the suggested viscosity range of 3-30 mPa·s, [13], the bioink demonstrated effective functionality throughout the printing process. To minimize variation and maximize biocapture molecule immobilization, a multilayered and overlapped pattern was employed, facilitating the immobilization of streptavidin and biotin-functionalized aptamer conjugates, as depicted in Fig. A.6(a). The number of printed layers was optimized by comparing the color intensity response of strips with a fixed S. typhimurium concentration (10<sup>6</sup> CFU mL<sup>-1</sup>). Tests ranging from 4 to 12 layers for test lines, and a fixed 8 layers for control lines, indicated that ten layers provided an optimal signal, as evidenced in Fig. A.6(b). This increased the availability of biocapture molecules, enhancing detection success. However, when exceeding this optimum 10-layer count, the "crowding effect" might hinder aptamer conformational changes, potentially suppressing signal response and resulting in high variation [9]. Initially, each deposition location received two ink droplets, resulting in a close distance between test and control lines. In subsequent experiments, only one droplet was deposited at each location.

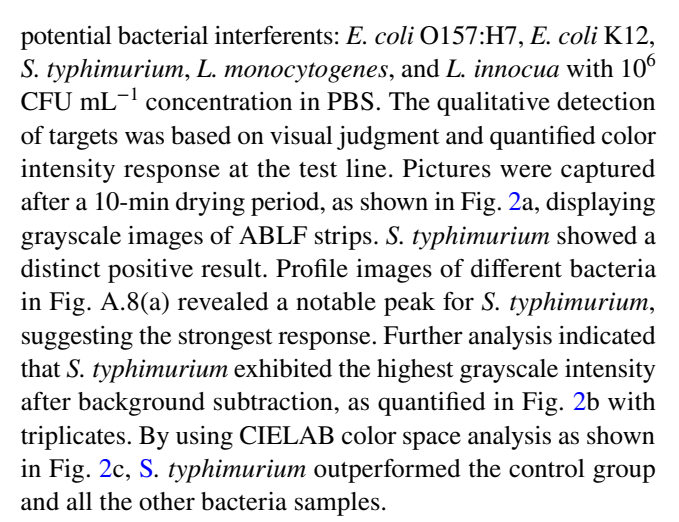
### Morphology and microstructure analysis

Top-view SEM imaging was performed to observe the capture of *S. typhimurium* and the flow of microparticles within the ABLF strips. After the standard preparation procedures, the ABLF strips underwent a 10-min drying period for SEM examination. The surface morphology and microstructure of the NC membrane, both with and without *S. typhimurium*, are depicted in Fig. 1. These micrographs illustrated the entrapment of microparticles by the complementary aptamer, as shown in Fig. 1h and i, which confirm proper liquid flow through the strip and the functionality of biocapture molecules on the control line.

Moreover, a comparison of the test region on the NC membrane before and after sample addition to the strips revealed significant morphological differences. In the absence of *S. typhimurium*, the original morphology of NC membrane appeared smooth surface in Fig. 1j. In contrast, the introduction of bacteria to the strips caused large aggregates to be trapped on the fibers of the NC membrane, creating a rough surface with numerous microparticles attached to the bacterial cells, as seen in Fig. 1k. Energy-dispersive X-ray spectroscopy (EDS) spectra were used to confirm the deposition of Ps-AuNPs-ssDNA, with six points selected for averaging in the provided figure, indicating 98.79 atomic percent (at%) of carbon (C) and 1.21 at% of gold (Au), as illustrated in Fig. A.7.

# Specificity and sensitivity of the aptamer-based lateral flow test strip

To evaluate the specificity of the ABLF strip developed in this study, five different microorganisms were examined as



The sensitivity of the ABLF assay was evaluated using *S. typhimurium* at concentrations ranging from 0 to 10<sup>7</sup> CFU mL<sup>-1</sup> by serial dilution. In Fig. 2d, image analysis showed a strong linear relationship between grayscale intensity and concentrations from 10<sup>2</sup> to 10<sup>6</sup> CFU mL<sup>-1</sup>, with a correlation coefficient of 0.978. Thus, the established LOD in PBS was 10<sup>2</sup> CFU mL<sup>-1</sup>, aligning with existing literature [10], with saturation noted at concentrations above 10<sup>6</sup> CFU mL<sup>-1</sup>. In CIELAB analysis, the sensitivity test with a range from 0 to 10<sup>7</sup> CFU mL<sup>-1</sup>, DeltaE results validated the previous conclusions from Fig. 2d, which presented linearity from 10<sup>2</sup> to 10<sup>6</sup> CFU mL<sup>-1</sup> concentrations as shown in Fig. 2e.

# Determination of foodborne pathogens in complex food samples

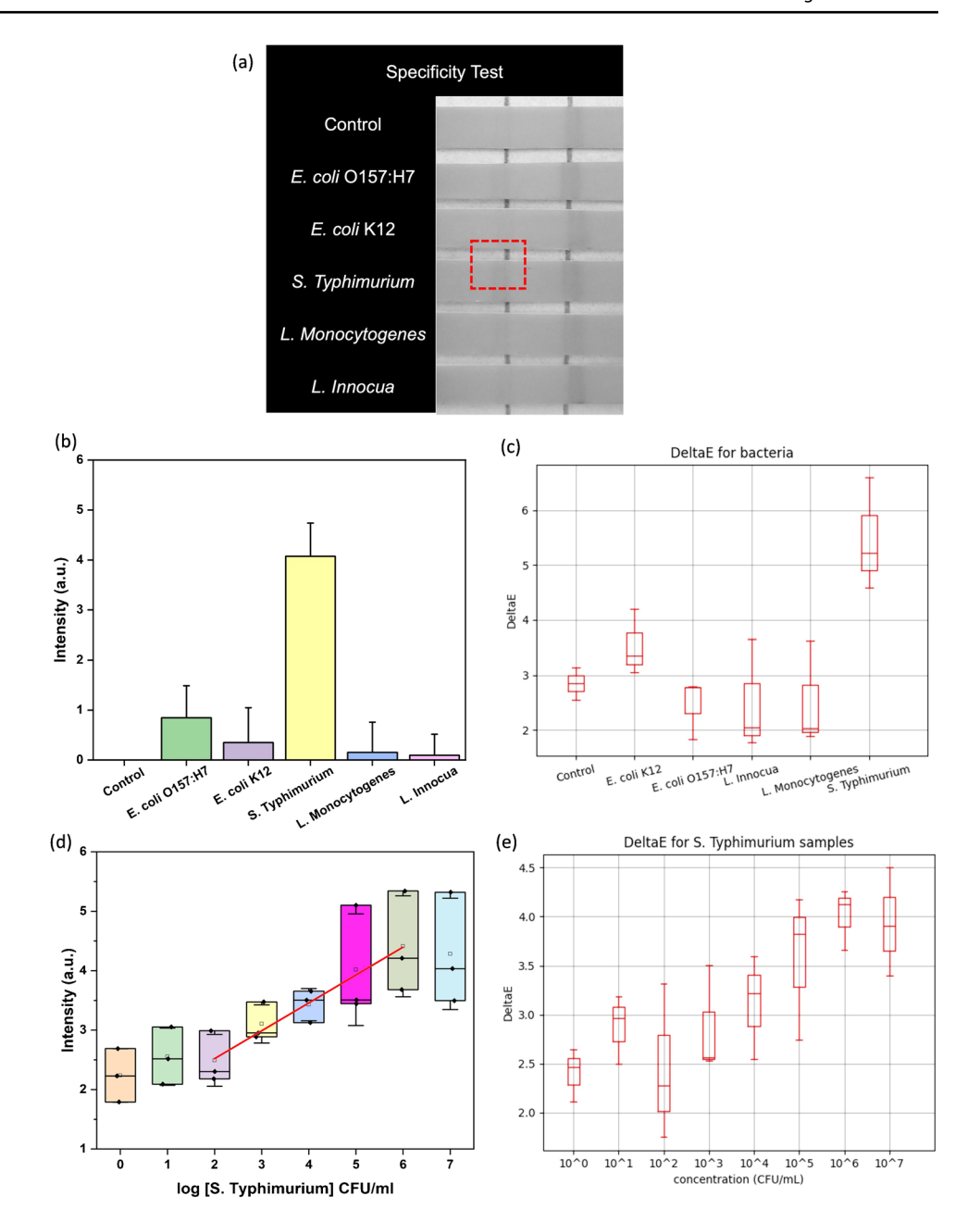
To demonstrate the real-world application of our ABLF platform for detecting S. typhimurium in real complex food samples, romaine lettuce was analyzed using our paperbased microfluidic device. S. typhimurium concentrations were tested from  $1.95 \times 10^2$  to  $1.95 \times 10^5$  CFU mL<sup>-1</sup>. The images in Fig. 3a indicated visible detection at  $1.95 \times 10^3$ CFU mL<sup>-1</sup>. Quantitative analysis showed high variability at this concentration level, as displayed in Fig. 3b, establishing the LOD in real sample detection at 10<sup>3</sup> CFU mL<sup>-1</sup>. Despite lower sensitivity compared to the PBS environment, due to sample interferences, the platform successfully detected S. typhimurium in complex samples with linearity from  $1.95 \times 10^2$  to  $1.95 \times 10^5$  CFU mL<sup>-1</sup>, as confirmed by a correlation coefficient of 0.9582, though more background noise was observed in real-sample testing, shown in Fig. A.9(a). The color space image processing method was applied to the same pictures from Fig. 3a. The sensitivity results in Fig. 3c observed a similar trend from 10<sup>2</sup> to 10<sup>5</sup> CFU mL<sup>-1</sup> as in Fig. 3b.

In past literature, few studies addressed the specificity of lateral flow devices in real-sample scenarios, especially for *S. typhimurium* in complex samples such as romaine lettuce



Microchim Acta (2024) 191:559 Page 9 of 13 **559** 

Fig. 2 Specificity and sensitivity test in PBS. a All interferent bacteria were tested at  $10^6$  CFU mL<sup>-1</sup>. The error bars show the standard deviation from the mean value. The quantitative results of the specificity test by **b** gray intensity difference and **c** CIELAB color space analysis. Correlation plot based on **d** gray intensity analysis and **e** CIELAB color space analysis results. The control group was tested in PBS



[12, 19, 32]. To demonstrate the specificity of our developed ABLF assays in real samples, *E. coli* O157:H7, *S. typhimurium*, and *L. monocytogenes* were tested. Utilizing 10<sup>4</sup> CFU mL<sup>-1</sup> for each bacterium, Fig. 3d illustrated a positive test result for *S. typhimurium* with the most prominent peak, indicating its suppression of the other bacteria. In the gray intensity profile, the highest peak confirmed the detection of *S. typhimurium*, as shown in Fig. A.9(b). Quantitative colorimetric data, adjusted for background noise and presented in Fig. 3e, indicated a positive correlation with these observations. CIELAB color space image analysis showed the large

gap of DeltaE between *S. typhimurium* and other bacteria samples confirming the specificity, as shown in Fig. 3f.

The spike-and-recovery assessment depicted in Fig. 3g verified our platform's efficacy, comparing favorably to traditional plate counting methods. With pathogen concentrations ranging from 10<sup>2</sup> to 10<sup>3</sup> CFU mL<sup>-1</sup>, recovery efficiency ranged from 92.8 to 97.4%. This validation underscored the inkjet printing system's ability to pattern aptameric ink on nitrocellulose membranes, while preserving the aptamers' molecular functionality, thus maintaining stable interaction with the target and mitigating interference from the food matrix.



**559** Page 10 of 13 Microchim Acta (2024) 191:559

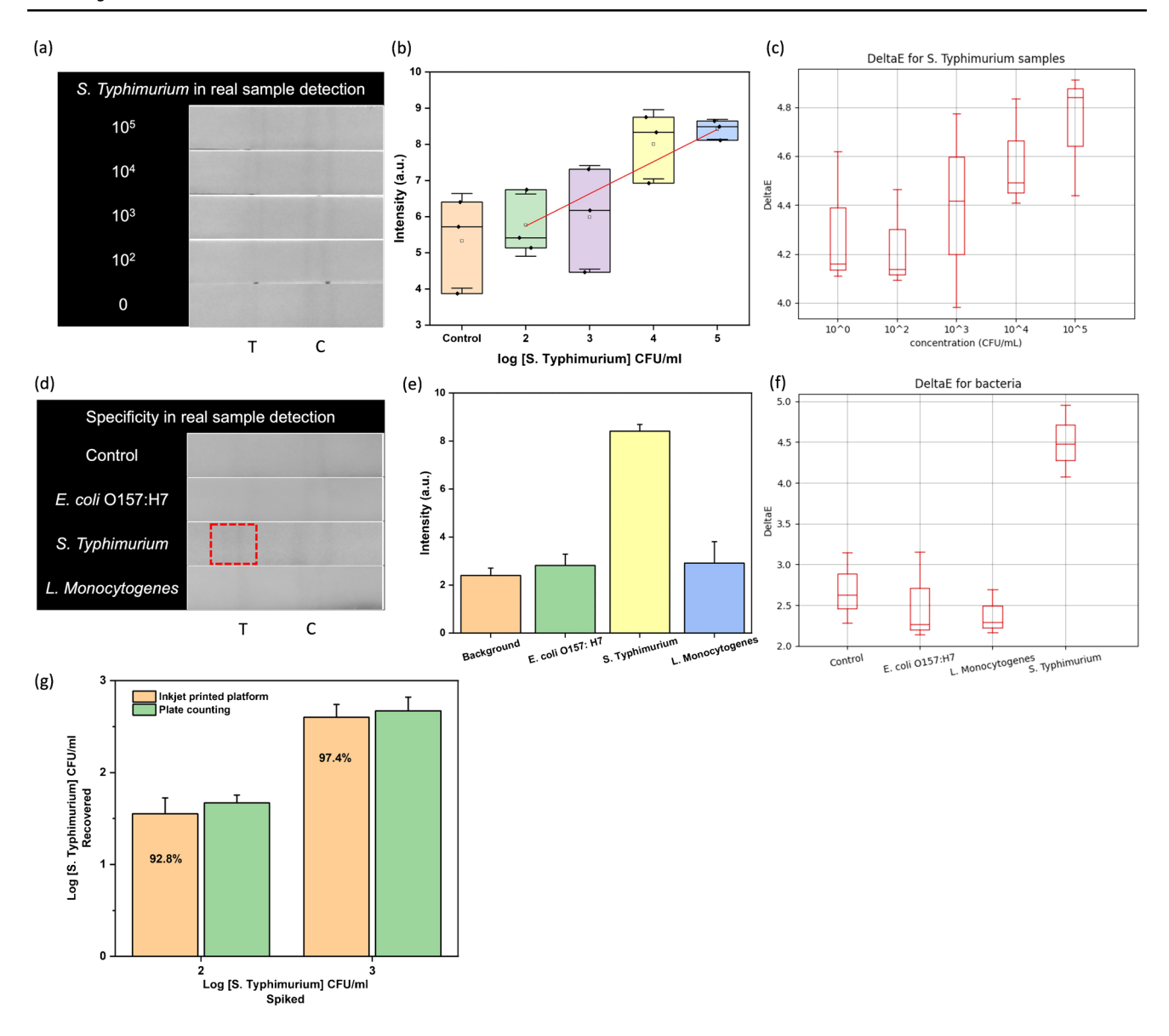


**Fig. 3** Real sample detection in romaine lettuce. In the sensitivity test, **a** images of *S. typhimurium* from  $10^2$  to  $10^5$  CFU mL<sup>-1</sup> compared with the control group. The quantitative results by **b** gray intensity difference analysis and **c** CIELAB color analysis with triplicates. In the specificity sensitivity test, **d** images of three different bacteria

with 10<sup>4</sup> CFU mL<sup>-1</sup>. The quantitative results by **e** gray intensity difference and **f** CIELAB color analysis to detect target bacteria in real samples. **g** Recovery performance of the proposed platform for detection of *S. typhimurium* from 10<sup>2</sup> to 10<sup>3</sup> CFU mL<sup>-1</sup>.

Upon thorough examination of the platform's efficacy, it exhibited improved performance in real sample conditions compared to previously reported chromatographic detection strategies for *S. typhimurium*, as outlined in Table 1. In the table, we list the probe signal and the LOD in both PBS and real sample conditions. Compared to other studies, our work demonstrated a low LOD of 10<sup>2</sup> CFU mL<sup>-1</sup> in PBS and 10<sup>3</sup> CFU mL<sup>-1</sup> in real samples. Additionally, while other works either use less complex samples, or a lower LOD for complex samples, our study is one of the few to report a low detection limit and high selectivity within the complex matrix of romaine lettuce.

### **Stability test**

Ensuring the ABLF assays' stability at room temperature is crucial, especially for field use in developing countries to avoid cold chain logistics. The ABLF strips, inkjet-printed and dried at 37 °C for 2 h, were stored at 4 °C and room temperature. They were tested for *S. typhimurium* detection (10<sup>7</sup> CFU mL<sup>-1</sup>) over 1, 14, 28, and 56 days. In each time, triplicates were performed to ensure the repeatability. The assays maintained over 91% of their activity after 56 days under both storage conditions, as shown in Fig. 4a and quantified in Fig. 4b.



Microchim Acta (2024) 191:559 Page 11 of 13 **559** 

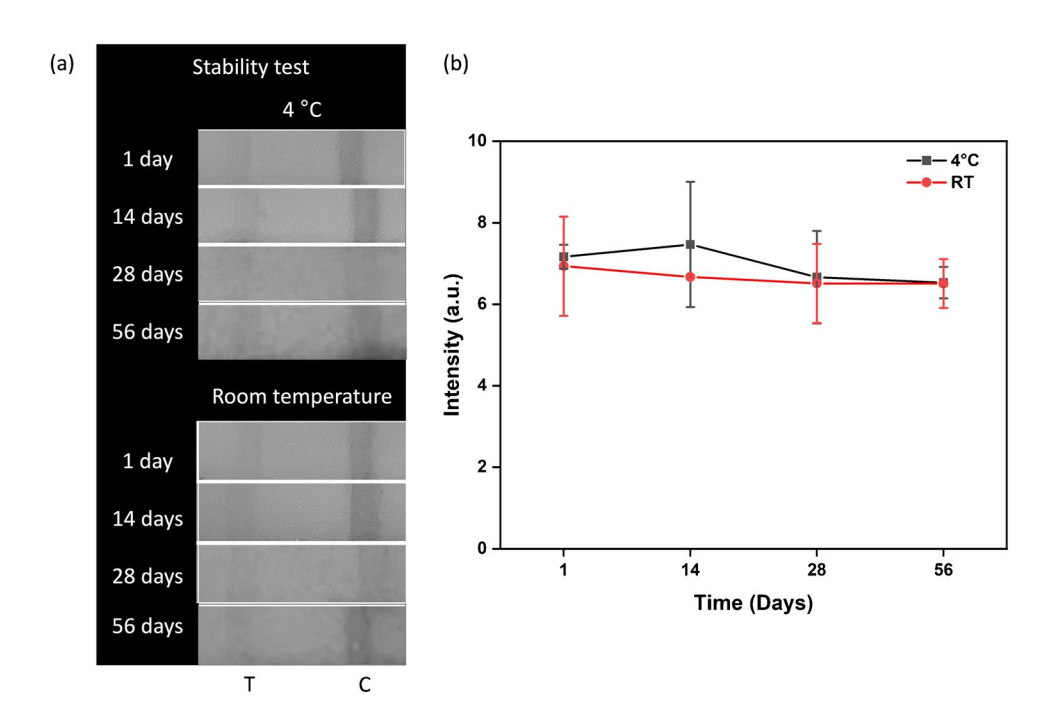
Table 1 Comparison of presented work with other reported lateral flow assays detection of S. typhimurium

Analytical method	Probe signal	LOD in PBS buffer (CFU mL <sup>-1</sup> )	LOD in real sample (CFU mL <sup>-1</sup> )	Selectivity in real sample (CFU mL <sup>-1</sup> )	Real sample	Ref
Colorimetric LFA	AuNPs <sup>a</sup> Au/MNCs	10 <sup>3</sup>	Not reported $10^3$	Not reported 10 <sup>5</sup>	Cooked food, chicken Milk	
Colorimetric-fluorescent-magnetic FLA	bCFMNs	Not reported $3.75 \times 10^3$	Not reported	Not reported	Milk, blood	[32] [33]
Up-converting phosphor LFA Colorimetric LFA	<sup>c</sup> UCPs <b>Ps-AuNPs</b>	10 <sup>4</sup> <b>10<sup>2</sup></b>	Not reported $1.95 \times 10^3$	Not reported $10^3$	Various foods Romaine lettuce	[34] This work

<sup>&</sup>lt;sup>a</sup>Au/MNCs, Gold-coated magnetic nanoparticle clusters

Data in bold emphasis indicates the results of this work

**Fig. 4** Stability test. **a** Grayscale images for 1, 14, 28, and 56 days. **b** The ABLF strips exhibit consistent performance after 56 days under both refrigeration at 4 °C and at room temperature



#### **Conclusion**

This study successfully introduced an inkjet-printed aptamer-based lateral flow platform for the detection of *Salmonella typhimurium*, which demonstrated good sensitivity and specificity. Utilizing grayscale intensity variation and CIELAB color space image processing, we achieved consistent and linear sensitivity in both buffer and real sample detection configurations. The strong affinity of the modified aptamer for *S. typhimurium* was confirmed through a host of quantitative analysis methods, including colorimetric assessments, TEM, and SEM imaging.

Our results indicate a detection limit of 10<sup>2</sup> CFU mL<sup>-1</sup> in PBS and 10<sup>3</sup> CFU mL<sup>-1</sup> in romaine lettuce samples. These results demonstrated the platform's high specificity and ability to distinguish pathogens in complex matrices. Additionally, the lateral flow device exhibited high selectivity for *S. typhimurium*, significantly outperforming other foodborne pathogens commonly tested. These findings underscore the robustness, low detection limit, extended stability, and high recovery rate of the ABLF platform, thus showing its potential for on-site food safety applications.

The insights obtained from this study will guide future optimization efforts. By exploring novel aptamer



<sup>&</sup>lt;sup>b</sup>CFMNs, Colorimetric-fluorescent-magnetic nanospheres

<sup>&</sup>lt;sup>c</sup>UCP, Up-converting phosphor particles

**559** Page 12 of 13 Microchim Acta (2024) 191:559

configurations and alternative functionalization techniques, we aim to further enhance the selectivity and detection performance of the sensor. These improvements are expected to expand the application scope of the sensor, increasing its utility in diverse food safety diagnostics.

**Supplementary Information** The online version contains supplementary material available at https://doi.org/10.1007/s00604-024-06633-5.

Author contribution Y.Y.: Conceptualization, Methodology, Validation, Formal analysis, Investigation, Writing – original draft, Writing – review & editing, Visualization. Z.W.: Methodology, Investigation. X.J.: Methodology, Formal analysis, Writing – original draft. E.W.: Methodology, Investigation, Writing – original draft. H.C.: Methodology, Validation. A.U.: Methodology. A.D.: Resources. G.C.: Resources, Validation, Supervision. J.A.: Validation, Supervision, Writing – review & editing. L.S.: Conceptualization, Resources, Data curation, Writing – original draft, Writing – review & editing, Validation, Supervision, Project administration, Funding acquisition.

**Funding** This work is supported by the US Department of Agriculture, Agricultural Research Service, under Agreement ARS-CFSE funding (no. 59–8072-6–001), project (no. 8072–42000-077-00D), and National Science Foundation (CBET award no 2127756).

**Availability of data and materials** No datasets were generated or analysed during the current study.

#### **Declarations**

**Ethical approval** This research did not involve human or animal samples.

Conflict of interest The authors declare no competing interests.

#### References

- Panich W et al (2024) Evaluation of semi-quantitative colorimetric assays based on loop-mediated isothermal amplification indicators by using image analysis. Anal Biochem 688:115481
- Scallan E et al (2011) Foodborne illness acquired in the United States—major pathogens. Emerg Infect Dis 17(1):7
- Havelaar AH et al (2015) World Health Organization global estimates and regional comparisons of the burden of foodborne disease in 2010. PLoS Med 12(12):e1001923
- Esmael A et al (2021) Isolation and characterization of two lytic bacteriophages infecting a multi-drug resistant Salmonella typhimurium and their efficacy to combat salmonellosis in ready-touse foods. Microorganisms 9(2):423
- Luo K, Kim H-Y, Oh M-H, Kim Y-R (2020) based lateral flow strip assay for the detection of foodborne pathogens: principles, applications, technological challenges and opportunities. Crit Rev Food Sci Nutr 60(1):157–170
- Hayashi T, Oshima H, Mashima T, Nagata T, Katahira M, Kinoshita M (2014) Binding of an RNA aptamer and a partial peptide of a prion protein: crucial importance of water entropy in molecular recognition. Nucleic Acids Res 42(11):6861–6875
- Wu J et al (2014) Recent trends in SELEX technique and its application to food safety monitoring. Microchim Acta 181:479–491
- Somvanshi SB et al (2022) Microfluidic paper-based aptasensor devices for multiplexed detection of pathogenic bacteria. Biosens Bioelectron 207:114214

- Díaz-Amaya S et al (2019) Inkjet printed nanopatterned aptamer-based sensors for improved optical detection of foodborne pathogens. Small 15(24):1805342
- Lu C, Gao X, Chen Y, Ren J, Liu C (2020) Aptamer-based lateral flow test strip for the simultaneous detection of Salmonella typhimurium, Escherichia coli O157: H7 and Staphylococcus aureus. Anal Lett 53(4):646–659
- Díaz-Amaya S, Lin L-K, Deering AJ, Stanciu LA (2019) Aptamer-based SERS biosensor for whole cell analytical detection of E. coli O157: H7. Anal Chim Acta 1081:146–156
- Gao P et al (2021) An enhanced lateral flow assay based on aptamer-magnetic separation and multifold AuNPs for ultrasensitive detection of Salmonella typhimurium in milk. Foods 10(7):1605
- Li X et al (2020) Inkjet bioprinting of biomaterials. Chem Rev 120(19):10793–10833
- Wyszecki G, Stiles WS (2000) Color science: concepts and methods, quantitative data and formulae, vol 40. John wiley & sons
- Liang Q et al (2022) Printed paper-based devices for detection of food-borne contaminants: new device design and new colorimetric image analysis methods. Electronic Imaging 34(15):371–375
- Zhao M, Diaz Amaya S, Jin S, Lin L-K, Deering AJ, Stanciu L, Chiu GTC, Allebach JP (2018) Inkjet printing platforms for DNAbased pathogen detection. NIP & Digital Fabrication Conference, no 1. Society for Imaging Science and Technology, pp 107–112
- Zhao M, Zhang R, Diaz-Amaya S, Lin L-K, Deering AJ, Stanciu L, Chiu GTC, Allebach JP (2019) Detection, imaging, and quantification of DNA-Based pathogen based on Inkjet-Printed test strips, NIP & Digital Fabrication Conference. Society for Imaging Science and Technology, pp 177–181
- Tasbasi BB, Guner BC, Sudagidan M, Ucak S, Kavruk M, Ozalp VC (2019) Label-free lateral flow assay for Listeria monocytogenes by aptamer-gated release of signal molecules. Anal Biochem 587:113449
- Wu Z (2019) Simultaneous detection of Listeria monocytogenes and Salmonella typhimurium by a SERS-based lateral flow immunochromatographic assay. Food Anal Methods 12:1086–1091
- Bhandari D, Chen F-C, Bridgman RC (2019) Detection of Salmonella typhimurium in romaine lettuce using a surface plasmon resonance biosensor. Biosensors (Basel) 9(3):94
- Duan N, Ding X, He L, Wu S, Wei Y, Wang Z (2013) Selection, identification and application of a DNA aptamer against Listeria monocytogenes. Food Control 33(1):239–243
- Liu J, Lu Y (2006) Preparation of aptamer-linked gold nanoparticle purple aggregates for colorimetric sensing of analytes. Nat Protoc 1(1):246–252
- Duda RO, Hart PE (1972) Use of the Hough transformation to detect lines and curves in pictures. Commun ACM 15(1):11–15
- Cao X, Ye Y, Liu S (2011) Gold nanoparticle-based signal amplification for biosensing. Anal Biochem 417(1):1–16
- Saha K, Agasti SS, Kim C, Li X, Rotello VM (2012) Gold nanoparticles in chemical and biological sensing. Chem Rev 112(5):2739–2779
- Lin L, Uzunoglu A, Stanciu LA (2018) Aminolated and thiolated PEG-covered gold nanoparticles with high stability and antiaggregation for lateral flow detection of bisphenol A. Small 14(10):1702828
- Jin S-A et al (2017) Gold decorated polystyrene particles for lateral flow immunodetection of Escherichia coli O157: H7. Microchim Acta 184:4879

  –4886
- Ulloa-Gomez AM, Agredo A, Lucas A, Somvanshi SB, Stanciu L (2023) Smartphone-based colorimetric detection of cardiac troponin T via label-free aptasensing. Biosens Bioelectron 222:114938



Microchim Acta (2024) 191:559 Page 13 of 13 **559** 

 Park SH, Kim J, Lee W-E, Byun D-J, Kim MH (2017) One-step synthesis of hollow dimpled polystyrene microparticles by dispersion polymerization. Langmuir 33(9):2275–2282

- Centi S, Tombelli S, Minunni M, Mascini M (2007) Aptamerbased detection of plasma proteins by an electrochemical assay coupled to magnetic beads. Anal Chem 79(4):1466–1473
- Barhoumi A, Zhang D, Halas NJ (2008) Correlation of molecular orientation and packing density in a dsDNA self-assembled monolayer observable with surface-enhanced Raman spectroscopy. J Am Chem Soc 130(43):14040–14041
- Hwang J, Kwon D, Lee S, Jeon S (2016) Detection of Salmonella bacteria in milk using gold-coated magnetic nanoparticle clusters and lateral flow filters. RSC Adv 6(54):48445–48448
- 33. Hu J et al (2018) Colorimetric-fluorescent-magnetic nanospherebased multimodal assay platform for Salmonella detection. Anal Chem 91(1):1178–1184

34. Zhao Y et al (2016) Rapid multiplex detection of 10 foodborne pathogens with an up-converting phosphor technology-based 10-channel lateral flow assay. Sci Rep 6(1):21342

**Publisher's Note** Springer Nature remains neutral with regard to jurisdictional claims in published maps and institutional affiliations.

Springer Nature or its licensor (e.g. a society or other partner) holds exclusive rights to this article under a publishing agreement with the author(s) or other rightsholder(s); author self-archiving of the accepted manuscript version of this article is solely governed by the terms of such publishing agreement and applicable law.

